Spectroscopy of Cu(II)-PcoC and the Multicopper Oxidase Function of PcoA, Two Essential Components of *Escherichia coli pco* Copper Resistance Operon[†]

David L. Huffman,[‡] Jennifer Huyett,[‡] F. Wayne Outten,[§] Peter E. Doan,[‡] Lydia A. Finney,[‡] Brian M. Hoffman,*[,‡,§] and Thomas V. O'Halloran*[,‡,§]

Department of Chemistry and Department of Biology, Molecular Biology, and Cell Biology, Northwestern University, Evanston, Illinois 60208

Received April 22, 2002; Revised Manuscript Received May 24, 2002

ABSTRACT: The plasmid-encoded *pco* copper resistance operon in *Escherichia coli* consists of seven genes that are expressed from two *pco* promoters in response to elevated copper; however, little is known about how they mediate resistance to excess environmental copper. Two of the genes encode the soluble periplasmic proteins PcoA and PcoC. We show here that inactivation of PcoC, and PcoA to a lesser extent, causes cells to become more sensitive to copper than wild-type nonresistant strains, consistent with a tightly coupled detoxification pathway. Periplasmic extracts show copper-inducible oxidase activity, attributed to the multicopper oxidase function of PcoA. PcoC, a much smaller protein than PcoA, binds one Cu(II) and exhibits a weak electronic transition characteristic of a type II copper center. ENDOR and ESEEM spectroscopy of Cu(II)-PcoC and the ^{15}N- and Met-CD_3-labeled samples are consistent with a tetragonal ligand environment of three nitrogens and one aqua ligand 'in the plane'. A weakly associated S-Met and aqua are likely axial ligands. At least one N is a histidine and is likely trans to the in-plane aqua ligand. The copper chemistry of PcoC and the oxidase function of PcoA are consistent with the emerging picture of the chromosomally encoded copper homeostasis apparatus in the *E. coli* cell envelope [Outten, F. W., Huffman, D. L., Hale, J. A., and O'Halloran, T. V. (2001) *J. Biol. Chem. 276*, 30670−30677]. We propose a model for the plasmid system in which Cu(I)-PcoC functions in this copper efflux pathway as a periplasmic copper binding protein that docks with the multiple repeats of Met-rich domains in PcoA to effect oxidation of Cu(I) to the less toxic Cu(II) form. The solvent accessibility of the Cu(II) in PcoC may allow for metal transfer to other plasmid and chromosomal factors and thus facilitate removal of Cu(II) from the cell envelope.

Copper is an essential element for cellular growth and is incorporated into a variety of proteins and enzymes. Copper salts are also potent antimicrobial and antifungal agents that are widely used to control plant pathogens (*1*). Wild-type *Escherichia coli* have several chromosomally encoded copper tolerance loci (*2*−*6*); however, organisms containing plasmid-based resistance genes are able to survive in significantly higher levels of environmental copper and are thus termed copper resistant (*7*). Copper resistance operons have been cloned and characterized from *Xanthomonas campestris*, *Pseudomonas syringae*, and *Escherichia coli* (*8*−*10*). Copper resistance in the *E. coli pco*[1] system is conferred by a plasmid containing at least seven genes that facilitate copper efflux (*11*, *12*). While several of these genes encode integral membrane proteins, none are members of known families of transporters. Two proteins are predicted to be soluble in the periplasm: PcoC, a small 103 aa protein, and PcoA, a 565 aa protein. PcoA bears some sequence similarity to the multicopper oxidases (*13*), including the yeast ferroxidase Fet3 (*14*, *15*), the human ferroxidase ceruloplasmin (*16*), ascorbate oxidase and laccase in plants, the manganese oxidase CumA in *Pseudomonas putida* (*17*), and the chromosomal multicopper oxidase CueO of *E. coli* (*18*, *19*).

Homologues of PcoA and PcoC from *Pseudomonas syringae* have been purified with bound copper (*20*); however, no biochemical assays or spectroscopic data are available. These proteins were proposed to protect the cells by sequestering copper, as has been proposed for the ability of yeast metallothionein to protect that organism from elevated copper concentrations. A hallmark of the bacterial copper resistance proteins PcoA and PcoC is the presence of methionine-rich sequence motifs, which are postulated to be involved in copper binding (*7*, *11*, *21*, *22*) (Figure 1). Methionine-rich domains similar to those in PcoC are also

[†] This work was supported by NIH Grants GM54111 (T.V.O.), HL13532 (B.M.H.), T32ES07284 (D.L.H.), and T32GM08061 (F.W.O.). L.A.F. acknowledges support as a Fellow of the Fannie and John Hertz Foundation.

* To whom correspondence should be addressed at the Department of Chemistry, Northwestern University, 2145 Sheridan Rd., Evanston, IL 60208. B.M.H.: Fax (847) 491-7713, Phone (847) 491-3104, E-mail bmh@northwestern.edu. T.V.O.: Phone (847) 491-5060, E-mail t-ohalloran@northwestern.edu.

[‡] Department of Chemistry.

[§] Department of Biology, Molecular Biology, and Cell Biology.

[1] Abbreviations: ENDOR, electron nuclear double resonance; ESEEM, electron spin−echo envelope modulation; EPR, electron paramagnetic resonance; *pco*, *Escherichia coli* plasmid-encoded copper resistance operon; *E. coli*, *Escherichia coli*; CDM, chemically defined medium; CFU, colony forming unit(s); IPTG, isopropyl β-D-thiogalactopyranoside.

10.1021/bi0259960 CCC: $22.00
Published on Web 07/10/2002

FIGURE 1: Methionine-rich domains of copper transporting proteins from yeast (yCTR1, accession number: NP_015449), rat (rCTR1, accession number: Q9JK41), and human CTR1 (hCTR1, accession number: O15431), with the *pco Escherichia coli* copper resistance proteins PcoA (accession number: s52253) and PcoC (accession number: s52255). Identical residues shown in black boxes, and regions of similarity are noted in gray boxes.

found in the CTR family of proteins essential for copper uptake in eukaryotes (*23, 24*).

PcoC bears no primary sequence homology to other structurally or functionally characterized copper-containing proteins. It is homologous to proteins from other copper resistance operons (*20, 25*); however, copper coordination chemistry has yet to be examined in any of these cases. Two of the three histidines of PcoC and all of the methionines are conserved among its homologues (Figure 2). PcoC may serve as a factor to present copper to PcoA or to escort copper out of the cell. A functional precedence for a metallochaperone function can be found in Atx1, a soluble 8 kDa copper trafficking protein in yeast (*26*). Atx1 shuttles copper to a homologous domain of the enzyme Ccc2 (*27*), a P-type ATPase that translocates copper across a vesicular membrane for eventual incorporation into Fet3 (*15*). Rae et al. have shown that the cytosol of eukaryotic cells has an overcapacity for copper chelation and typically maintains less than one free copper ion per cell (*28*). If a similar situation exists in prokaryotes, then a general function of the resistance pathway, including PcoA and PcoC, may be to maintain the cellular copper quota under conditions of copper excess through an export mechanism.

Here we demonstrate an essential role in vivo for both PcoA and PcoC by showing that inactivation of PcoC or PcoA causes cells to become more sensitive to excess environmental copper than wild-type cells. We also assign a multicopper oxidase function to PcoA, based on the copper-inducible oxidase activity of periplasmic extracts. In our model, PcoC acquires Cu(I) in the periplasm, then docks with PcoA, to effect oxidation to the less toxic Cu(II) form. Examination of the Cu(II)-loaded form of PcoC by ENDOR and EPR leads to a model for the coordination sphere of Cu(II)-PcoC. Together with genetic and biochemical assays of PcoA function, the data reveal a tightly coupled biochemical pathway and suggest a mechanism for this copper resistance pathway.

MATERIALS AND METHODS

Bacterial Strains and Plasmids. All manipulations were performed in *E. coli* following standard protocols(*29*). DH5α was used to store recombinant plasmids. The strains used for protein expression, BL21(DE3) and B834(DE3), and the plasmid pET11D were obtained from Novagen. Strain BW25113 was obtained from Dr. Barry Wanner (*30*). Plasmids pCOII36.15 (containing the gene for PcoC) and pCOVI104B1A (containing the full *pco* operon) were provided by G. Munson.

Growth Phenotypes of pco Mutants. To determine the copper growth phenotype of various *pco* constructs, the plasmids pSX34LacZα (low copy number null control, New England Biolabs), pcoVI104B1A (*pco*+), pcoII184A (Δ*pcoC*, codon 6 made a stop codon), and pcoI78 (Δ*pcoA*, deletion of codon 291 through codon 703) were transformed into strain DH5α. Cells were grown in 1XA minimal media (*31*), and plasmids were maintained with 30 μg/mL chloramphenicol. The *pco* mutant strains were grown to log phase and then serially diluted and plated on minimal agar plates containing various concentrations of copper sulfate. Colony forming units (CFU) were counted after 24 h of growth at 37 °C.

Construction of Vector for PcoC Overexpression. An overexpression vector for *pcoC* gene was prepared by the following method. A portion of the *pcoC* gene, without the leader sequence, was amplified by thermal cycling from the plasmid template, pCOII36.15, with primers 5′-GCT TTC TCT GCC ATG GCC CAT CCG GAA-3′ and 5′-CAG GAT CCT CAT AAT ATC ACT TCA CTG T-3′. These primers incorporated the unique restriction sites *Nco*I and *Bam*HI and also conserved the terminal codon of the leader sequence, thereby placing Ala at position 1 in the recombinant protein and His at position 2. The native protein contains His at position 1 of the sequence, preceded by the leader sequence MSILNKAILTGGLVMGVAFSAMA. The amplified gene was isolated, and then digested with *Nco*I and *Bam*HI; the resulting PcoC-encoding fragment was ligated into a similarly digested pET11D to produce pDLHII265.

Overexpression and Purification of PcoC. Cell cultures were grown at 37 °C in LB media containing 100 μg/mL ampicillin. A 10 L culture of BL21(DE3), transformed with pDLHII265, was grown aerobically to an OD_{600} of 0.6, and then protein expression was induced with IPTG. After 2 h, the cells were harvested by centrifugation, and the cell pellet was stored at −80 °C. The cell pellet was treated with three successive freeze/thaw cycles by freezing with liquid nitrogen

FIGURE 2: Alignment of plasmid-based copper resistance homologues from *Escherichia coli* PcoC (accession number: s52255), *Pseudomonas syringae* CopC (accession number: aaa25808), and *Xanthomonas campestris* (accession number: c36868), with a chromosomal open reading frame (orf) of *Escherichia coli* (accession number: 1788146). Identical residues shown in black boxes, and regions of similarity are noted in gray boxes. The bracket denotes the methionine-rich domain.

and then thawing at 25 °C. The pellet was resuspended in 240 mL of 10 mM Tris/MES, 25 mM NaCl, 1 mM EDTA at pH 8. After storage on ice for 1 h with periodic gentle agitation, the suspension was centrifuged at 6000*g* for 15 min at 4 °C. The pellet was discarded, and the supernatant was batch-treated with DEAE-Sephacel (Sigma, 0.4 mL of settled resin/mL of supernate) at pH 8, and then incubated for 30 min on ice with gentle stirring. The suspension was then filtered, and the DEAE-Sephacel was washed with 240 mL of 10 mM MES/Tris, 1 mM EDTA at pH 8, followed by filtration. The two filtrates were pooled, and the solution was adjusted to pH 6 with solid MES (Sigma). The solution was then loaded onto CM-Sepharose FF (Pharmacia, 1.6 cm × 24 cm). The protein was eluted with a linear NaCl gradient in 20 mM MES/Na, 0.1 mM EDTA, pH 6.0. The protein-containing fractions were pooled and concentrated with an Amicon device fitted with a YM-3 membrane. The typical yield of protein is ∼50 mg/L of culture. SDS−PAGE gel analysis confirmed that the protein was purified to a high degree of homogeneity. Electrospray mass spectrometry (ESI-MS) was performed by the University of Illinois Mass Spectroscopy Facility. The ESI-MS sample was prepared in a volatile buffer, 10 mM ammonium acetate (pH 6.6), and the final PcoC sample concentration was 136 mM. The MW determined by ESI-MS, 11 047, was within experimental error (±2 amu) of the expected value of 11 049.6. The isoelectric point (p*I*) of PcoC was determined to be greater than 9 using the Pharmacia Phast System fitted with a PhastGel IEF 3−9 gradient gel, consistent with the predicted p*I* of 10.22 using the algorithm Peptidesort in the computer program GCG, Wisconsin Package Version 10.1, Madison, WI.

Isotopic Labeling of PcoC. ^{15}N-Labeled PcoC was produced by growing BL21(DE3) cells transformed with pDLHII265 in 1 L of minimal media supplemented with [^{15}N]ammonium chloride as the sole nitrogen source. Minimal medium (M-^{15}N) consists of 6 g/L Na_2HPO_4, 3 g/L KH_2PO_4, 0.5 g/L NaCl, 1.0 g/L $^{15}NH_4Cl$, 0.4% glucose (w/v), and 2 mM $MgSO_4$. The procedure for protein expression was as follows: a 5 mL culture of BL21(DE3)/pDLHII265 was grown to saturation in LB with 100 μg/mL ampicillin (LB/Amp); then 125 mL of the saturated culture was inoculated into a fresh 5 mL tube of LB/Amp. The 5 mL culture was grown to an OD_{600} of 1.0 and centrifuged, and the cell pellet was resuspended in 5 mL of M-^{15}N medium and then added to 1 L of M-^{15}N in a 4 L flask. The cells were grown at 37 °C to an OD_{600} of 0.9, and expression was induced with IPTG. The cells were harvested 3 h later, and protein was isolated as described above, yielding 37 mg of pure protein.

To label the protein with CD_3-Met, protein expression was performed in the B834(DE3) Met auxotroph. The procedure for protein expression was as follows: a 5 mL culture of B834(DE3)/pDLHII265 was grown to saturation in M-Met medium which consists of 6 g/L Na_2HPO_4, 3 g/L KH_2PO_4, 0.5 g/L NaCl, 1.0 g/L $(NH_4)_2SO_4$, 40 mg/L Met, 0.4% glucose (w/v), and 2 mM $MgSO_4$. The saturated culture was used to inoculate a fresh 5 mL tube of M-Met containing CD_3-Met and grown overnight. This culture was used to inoculate 25 mL of M-Met containing CD_3-Met, and after 11 h of growth, it was added to 1 L of M-Met containing CD_3-Met. Once the OD_{600} reached 0.5, IPTG was added to induce protein expression. The cells were harvested 4 h later, and protein isolation was performed as described above to yield 45 mg of pure protein.

Preparation of Cu(II)-PcoC and Determination of Protein Concentration. The metalloprotein was prepared by adding 2 equiv of Cu(II)SO_4 per mole of PcoC in 10 mM HEPES/Na, 250 mM NaCl, pH 7.5. Excess metal was removed by repetitive washing with metal-free buffer in a Centricon-3 (Amicon). The final copper concentration was determined by ICP-AES. The protein concentration was determined by both A_{280} ($\epsilon = 8460\ cm^{-1}\ M^{-1}$) and the method of Bradford (*32*). The Bradford method, used to determine protein concentration, was modified by adding SDS to a final concentration of 0.005% in each sample, and a calibration curve was generated from a stock solution of PcoC. Both methods were calibrated by total amino acid hydrolysis, performed in triplicate by the University of Illinois Biotechnology Center. Generally, the A_{280} method gives values approximately 10% higher than the modified Bradford assay. The metal-to-protein ratio for all samples fell within the range of 0.8−1.2 mol of copper per mole of protein monomer.

Preparation of Cu(I)-PcoC and UV−Vis Analysis of Cu(I)- and Cu(II)-PcoC. The preparation of Cu(I)-PcoC was performed in a Vac Atmospheres anaerobic chamber under a nitrogen atmosphere. To 300 μL of 4.0 mM Cu(II)-PcoC in 50 mM HEPES/Na, pH 7.5, was added the reductant sodium ascorbate to a final concentration of ≈800 mM. The solution immediately bleached from purple to a pale yellow. The yellow color is due to oxidized ascorbate. The protein was then dialyzed extensively against 50 mM HEPES/Na, pH 7.5, to remove the reductant from the solution, first in a microdialysis cell and then with a Microcon-3 (Amicon) device. The final protein concentration was 1.83 mM with a metal-to-protein ratio of 0.9. The protein and metal ion concentrations were calibrated as described above for Cu(II)-PcoC. The UV−Vis spectra of Cu(I)- and Cu(II)-PcoC were collected with a Hewlett-Packard 8452 Diode Array Spectrophotometer. The Cu(I)-PcoC sample was removed from the anaerobic chamber in a sealed quartz cuvette for UV−Vis analysis.

Analytical Gel Filtration of Apo-PcoC and Cu(I)-PcoC. Analytical gel filtration was performed on a Superdex 75 HR 10/30 column at 4 °C using a BIO-RAD Biologic HR chromatography system. After equilibration in 10 mM HEPES, 250 mM NaCl, pH 7.5, 75 μL of 200 μM apo- or Cu(I) was injected onto the column. The samples were then eluted in 10 mM HEPES, 250 mM NaCl, pH 7.5, at a flow rate of 0.5 mL/min. The retention volume (V_e) of each peak was recorded. These retention volumes were then compared to a calibration curve of vitamin B_{12}, aprotinin, and RNase A where $(V_e - V_o)/(V_t - V_o)$ was plotted against the log of the molecular weight to give a straight line, V_o being the void volume of the column and V_t the bed volume of the column. Extinction coefficients at 280 nm of 8460 $M^{-1}\ cm^{-1}$ for apo-PcoC and 11 926 $M^{-1}\ cm^{-1}$ for Cu(I)-PcoC were used to normalize the two chromatograms.

Preparation of Periplasmic Extract. Overnight cultures of *E. coli* strain BW25113 and this strain transformed with a plasmid encoding the entire *pco* operon, pcoVI104B1A, were diluted 1:100 into 5 mL of Chemically Defined Medium (*3*). Cells were grown at 37 °C to an OD_{600} of 0.6−0.8, followed by addition of various concentrations of copper sulfate. After

1 h, the cells were harvested, and a periplasmic extract was prepared by the chloroform method (*33*). Briefly, the medium was drained, and the cells were resuspended into ~100 μL of remaining medium, followed by the addition of 50 μL of $CHCl_3$. After brief mixing, the cell suspension was incubated for 15 min at room temperature. Then 500 μL of 10 mM Tris/Cl, pH 8, was combined with the cell suspension to extract the released components of the periplasm. After centrifugation, the top layer, containing the periplasmic extract, was carefully removed and stored on ice, prior to the oxidase assays. Total protein concentration of the extract was determined by the method of Bradford (*32*).

Multicopper Oxidase Activity Assays. The activity assays were performed aerobically utilizing 3,3′-dimethoxybenzidine as the colorimetric indicator for oxidase activity at 25 °C (*34*). In the assay, 15 μL of periplasmic extract was combined with 225 μL of 0.1 M acetate/Na, pH 5.5. The reaction was initiated by the addition of 60 μL of 7.88 mM 3,3′-dimethoxybenzidine. The reaction was performed in duplicate for each assay, and the reactions were stopped at 5 and 120 min, respectively, by the addition of 600 μL of 18 N H_2SO_4 to each reaction. The difference in absorbance at 540 nm between the 120 and 5 min reactions was used to calculate the amount of oxidized substrate ($\epsilon = 9600\ \mu M^{-1}\ cm^{-1}$). A unit of activity is defined as micromoles of substrate oxidized per minute per milliliter of extract. The specific activity is defined as micromoles of substrate oxidized per minute per milligram of total protein in extract. All runs were performed in triplicate, and error bars represent ±1 standard deviation.

SOD Assays of Cu(II)-PcoC. The pyrogallol kinetic assay was performed in the following way based on published methods (*35*): 1.8 mL of 50 mM HEPES, 500 μM EDTA, pH 8.2, was combined either with 192 μL of MilliQ water for the control run or with 191 μL of MilliQ water and 1 μL of 2.39 mM Cu(II)-PcoC. The reaction was initiated by the addition of 8 μL of 10.1 mM pyrogallol in 0.1 M HCl. The kinetic reaction was monitored at 320 nm for 300 s for both the control assay and the assay with Cu(II)-PcoC. The standard cytochrome *c* kinetic assay was performed using previously described methods (*36*) at concentrations of 0, 0.02, 0.10, 1.0, and 10 μM Cu(II)-PcoC. No activity was observed by either method.

EPR and ENDOR Samples. All Cu(II)-PcoC samples for EPR and ENDOR studies were prepared in 30% glycerol. D_2O exchange was performed as follows: Cu(II)-PcoC in 10 mM HEPES/Na (pH 7.5), 250 mM NaCl was repetitively exchanged into D_2O-containing buffer. The deuterated buffer was prepared by three cycles of lyophilization and dilution of the original buffer into the same volume of D_2O (99.9%). This assured full exchange of buffer protons. Successive dilution and concentration of the protein sample with the deuterated buffer in a Centricon-3 device was performed until the D_2O was >97%. The final sample, 1.0 mM in PcoC, was combined with glycerol-d_3 (98%) to give a 30% glycerol (v/v) solution that was flash-frozen in liquid N_2 in a 600 μL quartz EPR tube.

EPR, ENDOR, and ESEEM Spectra. EPR spectra were taken at 77 K at X-band on an instrument previously described (*37*). ENDOR spectra were taken at 2 K in Q-band CW pulsed spectrometers described previously (*38, 39*). Some of the CW spectra were collected with a broad-band radio frequency (rf) irradiation produced by mixing the output of a PTS synthesizer with a Gaussian white-noise source of 100 kHz (*40*). Pulsed ENDOR spectra were collected using Mims (*41*) and Refocused Mims (ReMims) sequences (*42*). Stimulated echo 3-pulse ESEEM spectra were taken at 2 K in an X-band spectrometer described previously (*43*). X-band 3-pulse ESEEM time-domain spectra were Fourier-transformed into the frequency domain according to the method described by Mims (*44*).

A single-orientation ENDOR pattern has peaks at frequencies given to first order by

$$\nu_{\pm}^{(m)} = |\nu_n \pm \frac{A_n}{2} + \frac{3P_n}{2}(2m-1)|;\ m = 0,1 \qquad (1)$$

When A is small ($A < 2\nu_n$), the pattern is centered at ν_n (nuclear Larmor frequency) and split by the hyperfine interaction, A; otherwise, it is centered at $A/2$ and split by $2\nu_n$. Quadrupolar splitting ($3P$) is present for nuclei with a spin greater than 1/2. For comparison of spectra from isotopic nuclei, ^1H ($I = 1/2$) and ^2H ($I = 1$) nuclei, the coupling constants are related by the ratio of their Larmor frequencies (nuclear g factor). At 12 000 G, $\nu(^1H) = 51.1$ MHz and $\nu(^2H) = 7.8$ MHz.

$$\frac{A(^1H)}{A(^2H)} = \frac{\nu(^1H)}{\nu(^2H)} = 6.51;\ \frac{A(^{15}N)}{A(^{14}N)} = \frac{\nu(^{15}N)}{\nu(^{14}N)} = 1.403 \qquad (2)$$

Full interaction tensors can be obtained from frozen solutions by analysis of a set of ENDOR spectra collected at fields over the EPR envelope (*45, 46*). The EPR spectrum from a tetragonal Cu(II) usually has a large Cu hyperfine interaction ($A \sim 500$ MHz) arising from ^{63}Cu and ^{65}Cu isotopes. At X-band, the copper hyperfine splittings are comparable to the g-shift. However, when discussing proton and nitrogen ENDOR spectra taken at Q-band, to a good approximation one can ignore the $^{63,65}Cu$ hyperfine splittings because of the large field dispersion from g anisotropy, and can denote an observing field in terms of g value (*38*).

ENDOR and ESEEM Simulations. $^{14,15}N$ ENDOR and ^{14}N ESEEM simulations were performed using the approach described previously (*45*−*48*). The programs employed do not account explicitly to include the large $^{63,65}Cu$ hyperfine. Rather, to account for the copper hyperfine splittings, the simulations summed the calculation for four separate EPR envelopes, with each g corresponding to a separate branch of the four A splittings, so as to reproduce the observed experimental spectra (*47*).

RESULTS

Phenotypes of PcoA and PcoC Mutants. To establish the relative importance of the *pcoA* and *pcoC* in the *pco* operon, we disrupted each gene and measured the copper growth phenotypes of the mutant strains by serial dilution and colony formation. Surprisingly, we have discovered that in strains carrying the *pco* operon, disruption of *pcoC* causes a marked sensitivity to copper (Figure 3). While previous analysis of the *pco* operon revealed that *pcoC* is essential for copper resistance (*11*), the Δ*pcoC* strain, which still contains the *pcoA*, *pcoB*, and *pcoD* genes, is in fact *hypersensitive* to copper. Copper toxicity is much more pronounced in the Δ*pcoC* strain than in the *pco*$^-$ wild-type strain (Figure 3). We conclude that in the absence of *pcoC*, expression of the

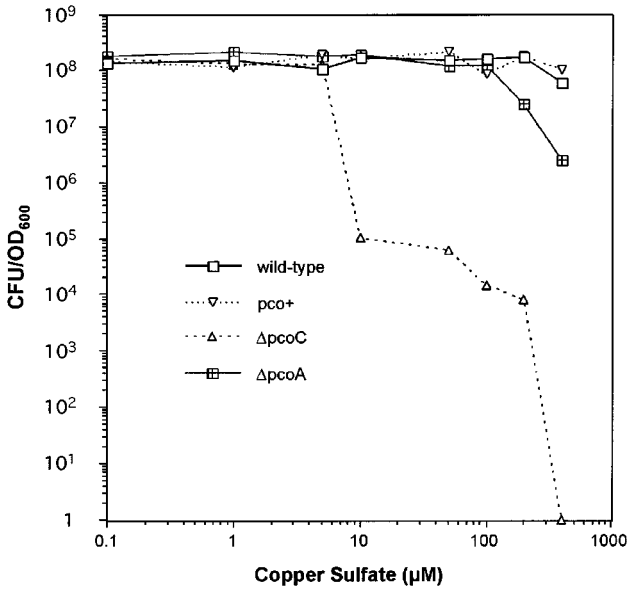

FIGURE 3: Growth phenotypes of wild type (DH5α *E. coli* with pSX34LacZα) (□), pco+ (DH5α *E. coli* with copper resistance plasmid pcoVI104B1A) (▽), ΔpcoC (DH5α *E. coli* with plasmid pcoII184A containing deletion of pcoC) (△), and ΔpcoA (DH5α *E. coli* with plasmid pcoI78 containing deletion of pcoA) (plus sign inscribed in open square) after plating onto minimal agar plates prepared with various concentrations of copper sulfate.

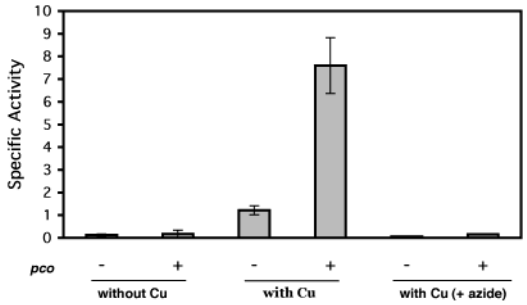

FIGURE 4: Oxidase assays of periplasmic extracts from wild-type strain and wild-type strain harboring the *pco* copper resistance plasmid. Activity was determined as described under Materials and Methods. Strains were grown with and without 200 μM copper sulfate in CDM media prior to isolation of periplasmic extracts. Sodium azide was added as described under Materials and Methods.

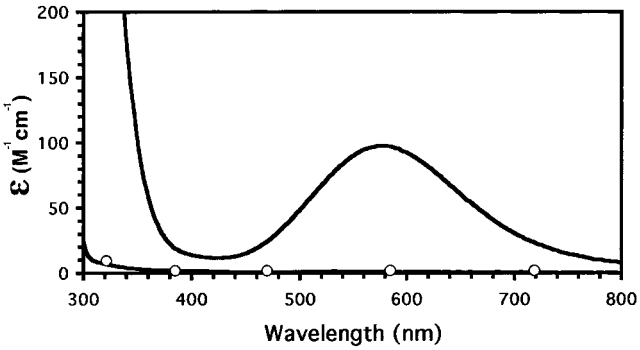

FIGURE 5: Optical spectra of Cu(II)-PcoC (—) and Cu(I)-PcoC (○) in 50 mM HEPES/Na, pH 7.5, at room temperature.

biochemical components of *pco* can prove deleterious to the cell, at otherwise tolerable copper stress. This result indicated that PcoC is a critical component in the copper resistance pathway and implies that it may interact with the other components of that pathway (i.e., PcoA, PcoB, and PcoD). Analysis of *pco* mutant constructs also reveals that deletion of *pcoA* causes a minor copper hypersensitivity phenotype (Figure 3). The Δ*pcoA* copper hypersensitivity is much less pronounced than that observed with Δ*pcoC*. This may be due to the fact that a copper-inducible homologue of PcoA known as CueO (copper export oxidase) is present in the *E. coli* chromosome (*18*, *19*). CueO activity may correct the otherwise severe effects of *pcoA* inactivation. The copper hypersensitivity observed when the *pco* operon is expressed in the absence of *pcoC* indicates that other components of *pco* may initiate damage to the cell envelope when PcoC is absent.

Oxidase Activity of Periplasmic Extracts. PcoA and PcoC contain N-terminal signal peptides that should direct secretion into the periplasm. The signal peptide of PcoA possesses the consensus motif SRRTFLK, which targets it for export by the *t*win-*a*rginine-*t*ranslocation (Tat) pathway. The Tat pathway is capable of transporting folded proteins across the cytoplasmic membrane into the periplasm (*49*, *50*). The signal sequence of PcoC is likely processed by Sec translocation machinery that can only act on unfolded proteins (*49*). Activity assays of periplasmic extracts of cells harboring the *pco* copper resistance operon reveal a copper-responsive oxidase activity (Figure 4). When the multicopper oxidase inhibitor sodium azide is added to the assay, the oxidase function of the periplasmic extract is eliminated. This oxidase activity above the wild-type background thus is attributed to the multicopper oxidase PcoA.

Spectroscopic Characteristics of PcoC. PcoC binds Cu(II) and readily forms with a 1:1 stoichiometry at physiological pH. Cu(II)-PcoC exhibits characteristics of the "normal" type II[2] copper environment (*51*). The Cu(II) form of PcoC exhibits a broad featureless absorption in the visible region with a maximum at 576 nm (100 M^{-1} cm^{-1}) which imbues the protein with a purple color (Figure 5). The electronic transition centered at 576 nm is absent in Cu(I)-PcoC. In contrast, bovine erythrocyte Cu,Zn-SOD possesses, relative to Cu(II)-PcoC, a maximum in the visible region at 680 nm (300 M^{-1} cm^{-1}) (*52*). Analytical gel filtration of apo-PcoC shows two peaks, one calibrating to approximately 16 kDa and a second calibrating to approximately 41 kDa (Figure 6). These two peaks are also seen in Cu(I)-PcoC; however, the area under the curve of the higher molecular weight peak increases by 68%, and the area of the lower molecular weight peak decreases by 23% in the Cu(I) case. Metal binding thus enhances the self-association of PcoC to form a higher order oligomeric state which is most likely a dimer. The apparent MW is somewhat higher than anticipated for spherically symmetric monomer; however, recent crystallographic data suggest that the apo-protein is quite oblate and this may account for the higher mobility (A. K. Wernimont, D. L. Huffman, T. V. O'Halloran, and A. C. Rosenzweig, manuscript in preparation). Given the oblate nature of the apo-protein, the copper-loaded form is also likely to have a large aspect ratio as well. In this case, the metal-induced oligomer is most likely a dimer.

The frozen solution EPR spectrum of Cu(II)-PcoC reveals an axial g tensor, $g = 2.21$ and 2.06, with $A_{\|}(Cu) = 195$ G,

[2] Using Kitajima's nomenclature (*68*), Cu(II)-PcoC is classified as type IIA, and Cu,Zn-SOD is classified as type IIC.

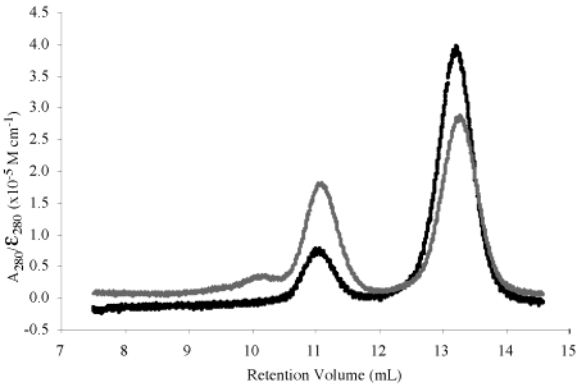

FIGURE 6: Analytical gel filtration of apo- and Cu(I)-PcoC. The chromatogram of apo-PcoC is shown in black, and that of Cu(I)-PcoC is shown in gray. The presence of two peaks in the chromatogram may indicate the transient formation of a higher molecular weight aggregate in the solution state.

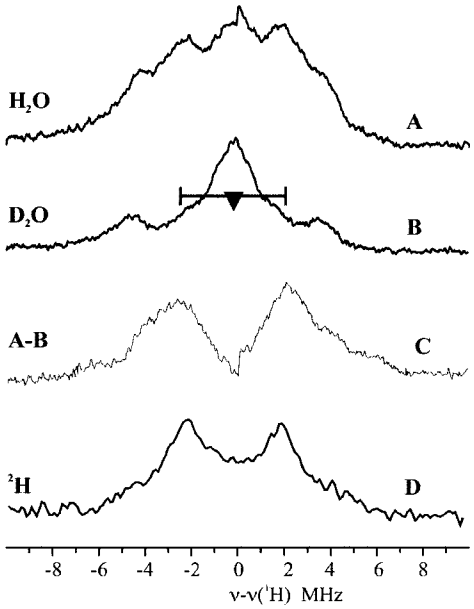

FIGURE 7: Pulsed and CW ^{1}H and ^{2}H ENDOR at $g = 2.28$. (A) ^{1}H CW ENDOR of the native sample; (B) ^{1}H CW ENDOR of D_2O exchanged; (C) difference of (A) and (B); (D) ^{2}H ReMims pulsed ENDOR scaled to ^{1}H's by nuclear g factor (eq 2). CW conditions: microwave power, 0.2 mW; microwave frequencies, (A) 34.943 and (B) 35.05 GHz; modulation amplitude, (A) 0.83 and (B) 1.07 G; scan rate, 1.0 MHz/s; number of scans, (A) 40 and (B) 55; rf power, 30 W; rf bandwidth, 60 kHz; and $T = 2$ K. Pulse conditions: $\pi/2$ pulse width = 60 ns; $\tau = 200$ ns; $\tau_{RF} = 60$ μs; repetition rate, 33 Hz; 20 shots per point; 10 scans; and $T = 2$ K.

whereas that of bovine erythrocyte Cu,Zn-SOD (*53*) is rhombic with g tensors of 2.03, 2.11, and 2.265 and $A_{||}$(Cu) = 130 G. To identify the ligands which form the active site of PcoC, we embarked on a series of ENDOR and ESEEM experiments to probe nuclei (^{1}H, ^{2}H, ^{14}N, ^{15}N) coupled to the metal center.

^{1}H ENDOR. ^{1}H ENDOR spectra demonstrate the presence of strongly coupled exchangeable protons. At the extreme low-field edge of the EPR spectrum (at a field at 35 GHz corresponding to a g-value of 2.28), the ^{1}H ENDOR spectrum of Cu(II)-PcoC (Figure 7A) shows a superposition of doublets centered at the ^{1}H Larmor frequency. When the protein is exchanged into D_2O, the ^{1}H ENDOR spectrum at $g = 2.28$ loses intensity, corresponding to a doublet with $A(^1\text{H}) \sim 5$ MHz (Figure 7B), as well as shoulders that correspond to a splitting of $A(^1\text{H}) \sim 10-12$ MHz. The difference spectrum (Figure 7C), obtained by subtracting Figure 7B from Figure 7A, highlights the intensity lost in the D_2O-exchanged sample. To help characterize these exchangeable protons, pulsed ^{2}H ENDOR was performed. The ^{2}H ENDOR spectrum at $g = 2.28$ matches the H_2O-D_2O proton pattern satisfactorily when scaled by 6.51, the ratio of the ^{1}H/^{2}H Larmor frequencies (Figure 7D).

The "single-crystal-like" ^{2}H pattern at $g = 2.28$ cannot be described in terms of a single type of proton. Recalling that an ENDOR pattern collected at $g_{||}$ has the external field normal to the bond of an in-plane ligand, but parallel to the bond of an axial ligand, comparison with the data for $[Cu(II)(H_2O)_6]^{2+}$ (*54*) suggests that the doublet with $A(^1\text{H}) \sim 5$ MHz corresponds to the protons of an equatorial H_2O/OH^-; the intensity with $A(^1\text{H}) \sim 10-12$ MHz is then plausibly assigned to an axial H_2O/OH^- (*54*). The field dependence ^{2}H ENDOR pattern (not shown) is consistent with this proposal.

^{14,15}N ENDOR. The ^{14}N CW ENDOR spectrum taken at $g_\perp$ (Figure 8) shows numerous features between 12 and 24 MHz and a shoulder to lower frequency (~10 MHz); this pattern cannot be assigned because it is a superposition of spectra from all orientations of the field within the $g_\perp$ plane and a single ^{14}N ($I = 1$) can give as many as 4 ν_+ peaks. The spectra should simplify at the low-field edge of the Cu(II) EPR envelope where the signal is from only one, "single-crystal-like" orientation, but this spectrum is broad and unresolved (data not shown).

To aid analysis, a sample was prepared with ^{15}N ($I = 1/2$), and the ^{15}N ENDOR field dependence (as shown in Figure 8) was collected. At $g_\perp$, the high-field edge of the EPR signal, the ^{15}N spectrum has a number of features between 16 and 33 MHz and a shoulder to lower frequencies (Figure 8). This pattern is best interpreted in terms of three inequivalent ^{15}N ligands, denoted as N1, N2, and N3. At $g = 2.28$, the low-field edge of the EPR signal, the ^{15}N ENDOR pattern coalesces into one large broad peak (~20−26 MHz) with a shoulder to higher frequency (at ~31 MHz). In the context of the full field dependence, the following assignments are proposed. The feature at ~31 MHz is present across the entire envelope and is assigned as the ν_+ branch of a ^{15}N1 doublet centered at $\nu_+ = \nu(^{15}\text{N}) + A/2$ [$A(^{15}\text{N1}) \approx 54$ MHz; $\nu(^{15}\text{N}) = 5.2$ MHz]. The ν_- partner would fall to lower frequency by $2\nu(^{15}\text{N}) = 10.4$ MHz, but is not seen; the absence of the ν_- feature is common in CW ENDOR. The marginally resolved features at 22 and 26 MHz in the "single-crystal-like" spectrum at $g = 2.28$ are assigned as the ν_+ branches from two additional nitrogens, N2 and N3, with $A(^{15}\text{N2}) = 43$ MHz and $A(^{15}\text{N3}) = 35$ MHz.

The three-dimensional, field versus frequency pattern of Figure 8 was simulated with these assignments, resulting in the following hyperfine coupling tensors: $a_{iso}(^{15}\text{N1}) = 54$ MHz; $A(^{15}\text{N2}) = [48, 42.6, 32]$; $a_{iso}(^{15}\text{N2}) = 41$ MHz; $A(^{15}\text{N3}) = [40, 34.6, 24.5]$; $a_{iso}(^{15}\text{N3}) = 33$ MHz. Scaling these hyperfine couplings by 1.40, and adding in small quadrupolar components ($3P_{max} = 2$ MHz) (*38*, *55*), gives a simulation that adequately describes features observed in the ^{14}N spectrum (Figure 8, top). The isotropic ^{14}N couplings, when scaled, are $a_{iso}(^{14}\text{N}) = 36$, 27, and 22 MHz for N1, N2, and N3, respectively.

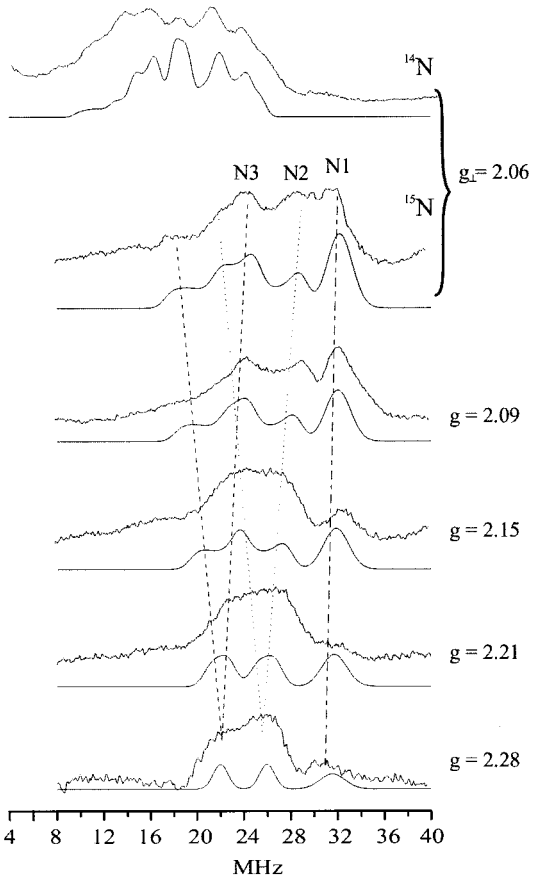

FIGURE 8: ^{14}N and ^{15}N CW ENDOR. Experimental conditions: microwave power, 2 mW; microwave frequency, 35.05 GHz (^{14}N), 35.027 GHz (^{15}N); modulation amplitude, 1.66 G; scan rate, 2 MHz/s; rf power, 25 W; $T = 2$ K; number of scans, 10 (^{14}N), 20 (^{15}N). Fields are indicated in the figure. Simulation conditions: $g_{||} = 2.28$; $g_\perp = 2.06$, 35.0 GHz; fields are as marked in the figure; EPR LW, 200 MHz. ^{14}N: $A(^{14}N1) = [24.7, 28.5, 17.5]$, $\alpha = \beta = 0$, $\gamma = 10°$; $A(^{14}N2) = [30.4, 34.2, 22.8]$, $\alpha = \beta = \gamma = 0$; $A(^{14}N3) = [38.2, 38.5, 38.5]$, $\alpha = \beta = \gamma = 0$; $P(^{14}N1) = P(^{14}N2) = P(^{14}N3) = [-1, -1, 2]$, ENDOR LW 1 MHz. ^{15}N: $A(^{15}N1) = [34.6, 40, 24.5]$, $\alpha = \beta = 0$, $\gamma = 10°$, ENDOR LW 1.5 MHz; $A(^{15}N2) = [42.6, 48, 32]$, $\alpha = \beta = \gamma = 0$, ENDOR LW 1.5 MHz; $A(^{15}N3) = [38.2, 38.5, 38.5]$, $\alpha = \beta = \gamma = 0$, ENDOR LW 2.5 MHz.

^{15}N-Pulsed ENDOR and ^{14}N ESEEM. To identify the nitrogen ligands, ^{15}N Mims pulsed ENDOR and 3-pulse ^{14}N ESEEM experiments were performed. Both techniques can reveal signals from the weakly hyperfine-coupled distal nitrogens of histidine ligands. Generally, the distal nitrogen of a histidine equatorially bound to Cu shows an isotropic coupling ~1/20 of the hyperfine coupling of the proximal nitrogen (*56*). Thus, the three strongly coupled ^{15}N would be expected to be accompanied by ^{15}N distal signals with weaker couplings, of ca. $a(^{15}N) \sim 2.7$, 2.0, and 1.6 MHz, if all three were from histidine; however, this factor of "20" is far from a precise value. ^{15}N Mims ENDOR spectra at $g = 2.06$ give a well-resolved doublet of $A(^{15}N4) = 2.3$ centered at $\nu(^{15}N)$, and a second doublet of $A(^{15}N5) \sim 0.9$ MHz (Figure 9), plus intensity with yet smaller couplings. The ^{15}N4 coupling is of appropriate magnitude to be assigned to the distal nitrogen(s) of one or more equatorially bound histidines, whose proximal nitrogens are N1 and N2. The coupling to N5 is somewhat smaller than expected. Nonetheless, it is most plausible that both correspond to the remote nitrogen of a histidine. The observation of two doublets which likely arise from the remote nitrogen of a Cu-bound histidine would imply the presence of no fewer than two histidyl ligands.

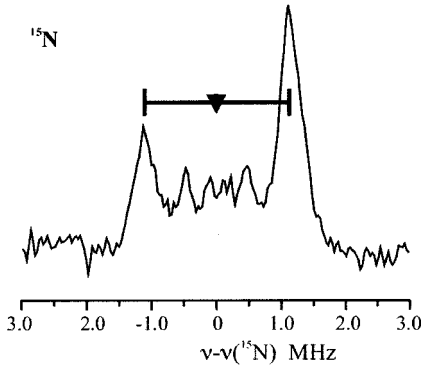

FIGURE 9: ^{15}N Mims pulsed ENDOR at $g = 2.06$. Conditions: microwave frequency, 34.743 GHz; $T = 2$ K; $\pi/2$ pulse width = 80 ns; $\tau = 268$ ns; $\tau_{RF} = 60$ μs; repetition rate, 33 Hz; 20 shots per point; 6 scans.

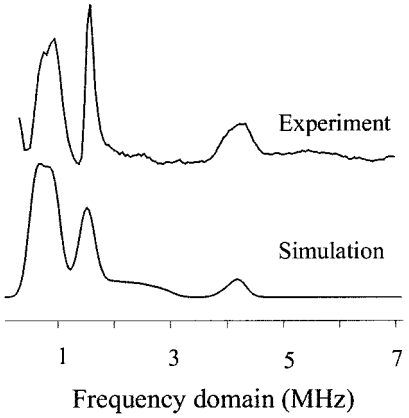

FIGURE 10: ^{14}N 3-pulse ESEEM of Cu(II)-PcoC shown in the frequency domain with simulation. Experimental conditions: microwave frequency, 9.410 GHz; $T = 4$ K; repetition rate, 33 Hz; 20 shots per point; $\tau = 168$ ns; $\pi/2$ pulse width = 16 ns; $g = 2.06$; 4 scans; 256 points; resolution, 40 ns; and start time = 0.128 μs. Simulation conditions: $A = [1.95, 1.85, 2.05]$ and $P = [-0.1, 0.81, -0.71]$ MHz; 512 points; resolution, 40 ns; and all other conditions are the same as in the experiment. Fourier transform of time domain (not shown), experimental and simulation, obtained by dead time reconstruction patterned after Mims (*44*).

It is also possible that the doublet with the larger coupling and broader lines in fact arises from overlapping signals from two similar histidyl ligands. To test this possibility, we performed X-band ESEEM measurements: ^{14}N ESEEM at X-band is very sensitive to the number of weakly coupled remote ^{14}N of His bound to a copper center when the hyperfine coupling is of the magnitude of N4 (ESEEM is not sensitive to a nitrogen with the coupling seen for N5) (*57*). Figure 10 (top) is the 3-pulse ESEEM spectrum obtained at $g = 2.06$ for Cu(II)-PcoC. We assign the peaks below 2 MHz to the ^{14}N spin manifold where the hyperfine and nuclear Zeeman interaction oppose each other as follows: ν_0 and ν_- contribute to the broad peak at 0.8 MHz, and ν_+ is the sharp peak at 1.5 MHz. The broad weaker peak at ~4 MHz is ν_{DQ}, the "double quantum" transition from the other electron spin manifold (*57*−*59*). Using these assignments, we simulated the ESEEM spectra with a single remote ^{14}N4 and the following parameters: $K = 0.41$ MHz, $\eta = 0.83$ (the asymmetry parameter), and $a_{iso}(^{14}N4)_{ese} \sim 2.0$

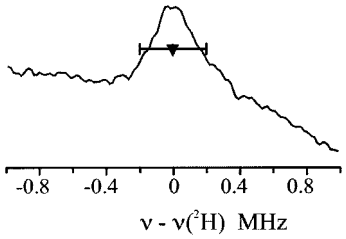

FIGURE 11: ^{2}H Mims pulsed ENDOR of CD_3-methionine. Conditions: microwave frequency, 34.663 GHz; temp = 2 K; $\pi/2$ pulse width = 80 ns; τ = 700 ns; τ_{RF} = 60 μs; repetition rate, 33 Hz; 20 shots per point; 6 scans.

MHz.[3] This simulation agrees well with the experiment (Figure 10) and with literature values (*57*, *60*−*62*). These values, most particularly the quadrupole constants, show that this nitrogen is indeed the remote distal nitrogen of a bound histidyl imidazole.

In addition, simulations of the ESEEM with two or three equivalent distal N4 nitrogens give strong combination features at 2−3 MHz, which are absent in the experimental spectrum. We conclude that the coordinated N1 corresponds to the proximal nitrogen of a single histidine whose remote nitrogen is N4. The coupling to a ^{14}N5, as predicted from the ^{14}N5 coupling measured by ENDOR, is too small to expect any significant modulation, at either fundamental or combination frequencies.

The ^{15}N-pulsed ENDOR spectra show that there are other weakly coupled ^{15}N and the values for $a_{iso}(^{14}N)$ would be ∼0.6 MHz and less, when scaled from the ^{15}N values. In the presence of ^{14}N4, ESEEM from such nitrogens also would be too weak to detect. Thus, it is not possible to determine the ^{14}N quadrupole constants from these other weakly coupled nitrogens to prove whether they are from histidine.

CD_3-Methionine. To test the possibility that Met is a ligand in Cu(II)-PcoC, we labeled the protein with CD_3-methionine and performed ^{1,2}H ENDOR experiments. ^{1}H ENDOR did not show any visible loss of intensity relative to the unlabeled sample. A ^{2}H ENDOR spectrum taken at $g_\perp$ does, however, show a single broad peak centered at $\nu(^2H)$, with a total breadth of $A(^2H)$ = 0.6 MHz (Figure 11). This pattern narrows at the lower fields, $A(^2H) < 0.4$ MHz. This pattern is assigned as arising from a distribution of rotamers from the CD_3 group of methionine. The breadth of the pattern is comparable to that seen for CD_3 of azurin (Doan, P., and Hoffman, B. M., unpublished experiments), and is such that a point−dipole interaction with the copper spin corresponds to a range of values for the shortest Cu−D distance of 3.5−3.9. This range of Cu−D distances is consistent with the reported values for Cu−S (Met) distances (2.62−3.11 Å) in blue copper centers (*63*). Therefore, the data are consistent with the sulfur of methionine as at least one of the two axial ligands to the Cu(II) center.

DISCUSSION

These results demonstrate that *pcoC*, a gene essential for *pco*-mediated copper resistance (*7*, *11*), encodes a protein that binds a single Cu(II) ion per monomer and that copper binding can induce formation of higher order oligomers. This is in contrast to the well-established copper detoxification protein yeast metallothionein, which functions to protect the cell by sequestering over seven or more copper ions per monomer. The Cu-hypersensitivity phenotype of the *pcoC*-null cells indicates that PcoC protein must work within a biochemical pathway to allow the bacterium to survive under conditions of copper excess. These genetic results suggest that one function may involve a partnership with the protein encoded by the *pcoA* gene, shown here to be a multicopper oxidase. While the exact roles of PcoC and PcoA in the *E. coli* copper resistance mechanism have yet to be established, spectroscopic and biochemical data on the solvent-accessible Cu(II) site described below are consistent with a metal-transfer function reminiscent of the Atx1 metallochaperone (*26*), an electron-transfer function, or both.

Spectroscopy of the Cu(II) Site. EPR, ENDOR, and ESEEM spectra of Cu(II)-PcoC are unusually broad, even for a Cu(II) protein center, suggesting that the Cu(II) site is not well organized. The site may be characterized as an unusually broad distribution of conformers/microstates. Nonetheless, inferences can be drawn as to the average structure of this site. The EPR spectrum of Cu(II)-PcoC gives parameters of $g_{||} = 2.21$ and $A_{||} = 546$ MHz, in the expected range for a type II copper center with 2−4 equatorial N donors and 1−2 O donors (*51*). CW ^{1}H and pulsed ^{2}H ENDOR data indicate the presence of exchangeable protons from an equatorial H_2O/OH^- ligand, and suggest the possibility of a second water not in the plane, perhaps as a weak axial ligand. Because of the complexity and spectral overlap in the ^{14}N CW ENDOR spectra, the protein was fully labeled with ^{15}N and ^{15}N CW ENDOR was performed. A simulation of the full field-frequency ^{15}N ENDOR pattern collected at intervals across the EPR envelope suggests the presence of three distinct equatorial nitrogens, N1, N2, and N3, with nearly isotropic couplings, where $a_{iso}(^{14}N) \sim 36$, 27, and 22 MHz, respectively. These ^{14}N couplings are similar to those reported for other copper proteins with histidyl nitrogens as ligands (*64*, *65*), and are quite consistent with copper sites containing three N ligands. As N1 is distinctly different from N2 and N3, we speculate that N1 is trans to the in-plane aqua ligand.

^{15}N ENDOR discloses signals from two additional weakly coupled ^{15}N that have been tentatively assigned as the remote nitrogens of bound histidyl imidazoles. Stimulated Echo ESEEM of natural-abundance protein and Mims Pulsed ENDOR of ^{15}N-labeled protein confirm that at least one of these is indeed from histidine. Together, the two approaches give evidence supporting the idea that two of the copper ligands are from histidine.

Cu(II)−Methionine Interaction. PcoC has a Met-rich motif, $MX_2MX_2MX_2HX_2M$, similar to ones found in other copper resistance proteins such as PcoA and copper trafficking proteins such as Ctr family members (Figure 1). To test for Cu(II)−S(Met) interactions, PcoC was selectively labeled with Met-CD_3, and ^{2}H Mims Pulsed ENDOR was performed. A coupling with a breadth of ∼0.6 MHz at $g_\perp$ is consistent with the assignment as a distribution of rotamers. Using a point−dipole model, an estimate of the shortest Cu−D distance is 3.5−3.9 Å. These distances are consistent with the Cu−methyl proton distance in type I blue copper sites where the Cu−S(Met) distances are indicative of methionine

[3] This ^{14}N coupling is significantly different from that obtained by scaling A(15N5) obtained from pulsed ENDOR. Such a discrepancy has been reported recently by others (*69*).

ligation (*66*). While the sulfur of methionine in this model is close enough to be a Cu(II) ligand, these methods cannot reveal direct Cu−S interaction. Thus, a close packing but nonbonding interaction between a Met side chain and Cu(II) can also explain the ENDOR data.

Biochemical Properties and Functional Insights. The Cu(II) form of the protein has at least one exogenous ligand and can be reduced by physiological reducing agents such as ascorbate to Cu(I). The Cu(II) site in PcoC is classified as type II[2], like that of Cu,Zn-SOD1; however, Cu-PcoC does not exhibit superoxide dismutase activity in either the standard kinetic cytochrome *c* assay or the pyrogallol kinetic assay. While other catalytic activities are possible, the results here are consistent with the two proposed mechanisms by which PcoC works in partnership with the oxidase, PcoA. The tetragonal ligand environment of PcoC is unlike that of other enzymes with mononuclear copper sites, since it contains no cysteine or tyrosine ligands or other cofactors. A priori, the function of an enzyme or protein cannot be predicted from the ligand environment alone; however, the methionine-rich domain (Figure 1) of PcoC and the homologous domain contained in PcoA implicate a function in copper efflux, analogous to that of the eukaryotic Ctr family of proteins (*23*). In addition, a homologue of PcoA, CueO, located on the *E. coli* chromosome is essential for aerobic copper tolerance and also displays a copper inducible oxidase activity (*18*).

As an analogy with the Atx1 copper chaperone (*67*), which delivers its metal ion cargo to the homologous domains of a copper processing enzyme, *Ccc*2, we propose a model in which Cu(I)-PcoC functions as a copper chaperone that docks with the multiple repeats of Met-rich repeats of PcoA. The Cu(I) delivered by PcoC to PcoA would not become one of the catalytic coppers of the multicopper oxidase, but would rather be a source of reducing equivalents for the PcoA enzyme. A precedent for a transition metal acting as a substrate that provides reducing equivalents to an oxidase can be found in the ferroxidase activities of ceruloplasmin and Fet3, multicopper oxidases which can catalyze the oxidation of Fe(II) (*16*). In the case of PcoA, oxidation would convert Cu(I) to the less toxic Cu(II) form (*18*) that could be subsequently conducted to other proteins in the copper resistance pathway for export across the outer cell wall. Other functions cannot be ruled out. For instance, the copper-loaded form of PcoC may simply serve to catalyze electron transfer to the O_2-dependent multicopper oxidase, and PcoA or PcoC may serve as a shuttle to deliver Cu(I) to an outer membrane component like PcoB. In the latter scenario, PcoA might contribute to the resistance by acting as a terminal oxidase that energizes membrane-bound copper transport proteins.

Concluding Remarks. The EPR, ENDOR, and ESEEM results demonstrate that the Cu(II) of Cu(II)-PcoC has a tetragonal ligand environment with an aqua (OH_x) ligand 'in the plane'. The spectroscopy suggests the three remaining in-plane ligands are nitrogenous. ENDOR and ESEEM combine to show that one is from histidine. ENDOR suggests it is likely that a second is as well. The data do not address the identity of a third nitrogenous ligand, and thus admit to it having a different origin. We note that there are sufficient His in the amino acid sequence of PcoC to account for three ligands. These His are widely spaced throughout the primary structure, but only two are conserved in homologues from other copper resistance operons. Furthermore, the Cu(II)-bound histidines may come from adjacent monomers within a metal-bridged PcoC oligomer. A weakly bound S-Met and aqua are potential axial ligands. We postulate that a histidine N1 is trans to the in-plane aqua ligand. These results suggest that the copper is quite accessible to solvent, and presumably available to partner proteins. In the absence of a definitive PcoC activity, the question of which oxidation state and oligomerization state are active in vivo remains open. Clearly, *E. coli* have developed complex trafficking pathways to control the reactivity of excess copper ions in both the periplasm and cytoplasm of the cell (*18*, *19*). This work establishes that the mechanism of copper resistance requires copper cofactors to alleviate copper stress and that both a multicopper oxidase, PcoA, and a copper-binding protein, PcoC, are crucial for copper resistance. It is becoming clear that cells minimize the activity of free copper ions regardless of the abundance or availability of copper in the extracellular medium.

REFERENCES

1. Millardet, P. M. A. (1885) *J. Agr. Prat. 2*, 801−805.
2. Munson, G. P., Lam, D. L., Outten, F. W., and O'Halloran, T. V. (2000) *J. Bacteriol. 182*, 5864−5871.
3. Outten, F. W., Outten, C. E., Hale, J., and O'Halloran, T. V. (2000) *J. Biol. Chem. 275*, 31024−31029.
4. Stoyanov, J. V., Hobman, J. L., and Brown, N. L. (2001) *Mol. Microbiol. 39*, 502−511.
5. Petersen, C., and Moller, L. B. (2000) *Gene 261*, 289−298.
6. Rensing, C., Fan, B., Sharma, R., Mitra, B., and Rosen, B. P. (2000) *Proc. Natl. Acad. Sci. U.S.A. 97*, 652−656.
7. Bryson, J. W., O'Halloran, T. V., Rouch, D. A., Brown, N. L., Camakaris, J., and Lee, B. T. O. (1993) in *Bioinorganic Chemistry of Copper* (Karlin, K., and Tyeklar, Z., Eds.) pp 101−105, Chapman & Hall, New York.
8. Rouch, D., Camakaris, J., Lee, B. T., and Luke, R. K. (1985) *J. Gen. Microbiol. 131*, 939−943.
9. Bender, C., and Cooksey, D. (1987) *J. Bacteriol. 169*, 470−474.
10. Lee, Y., Hendson, M., Panopoulos, N. J., and Schroth, M. N. (1994) *J. Bacteriol. 176*, 173−188.
11. Brown, N. L., Barrett, S. R., Camakaris, J., Lee, B. T., and Rouch, D. A. (1995) *Mol. Microbiol. 17*, 1153−1166.
12. Rouch, D. A., and Brown, N. L. (1997) *Microbiology 143*, 1191−1202.
13. Solomon, E. I., Sundaram, U. M., and Machonkin, T. E. (1996) *Chem. Rev. 96*, 2563−2605.
14. Askwith, C., Eide, D., Van Ho, A., Bernard, P. S., Li, L., Davis-Kaplan, S., Sipe, D. M., and Kaplan, J. (1994) *Cell 76*, 403−410.
15. Yuan, D. S., Stearman, R., Dancis, A., Dunn, T., Beeler, T., and Klausner, R. D. (1995) *Proc. Natl. Acad. Sci. U.S.A. 92*, 2632−2636.
16. Kaplan, J., and O'Halloran, T. V. (1996) *Science 271*, 1510−1512.
17. Brouwers, G. J., de Vrind, J. P., Corstjens, P. L., Cornelis, P., Baysse, C., and de Vrind-de Jong, E. W. (1999) *Appl. Environ. Microbiol. 65*, 1762−1768.
18. Outten, F. W., Huffman, D. L., Hale, J., and O'Halloran, T. V. (2001) *J. Biol. Chem. 276*, 30670−30677.
19. Grass, G., and Rensing, C. (2001) *J. Bacteriol. 183*, 2145−2147.
20. Cha, J. S., and Cooksey, D. A. (1991) *Proc. Natl. Acad. Sci. U.S.A. 88*, 8915−8919.
21. Voloudakis, A. E., Bender, C. L., and Cooksey, D. A. (1993) *Appl. Environ. Microbiol. 59*, 1627−1634.
22. Cooksey, D. A. (1994) *FEMS Microbiol. Rev. 14*, 381−386.
23. Pena, M. M., Lee, J., and Thiele, D. J. (1999) *J. Nutr. 129*, 1251−1260.
24. Pena, M. M., Puig, S., and Thiele, D. J. (2000) *J. Biol. Chem. 275*, 33244−33251.
25. Lee, Y. A., Hendson, M., Panopoulos, N. J., and Schroth, M. N. (1994) *J. Bacteriol. 176*, 173−188.

26. Pufahl, R. A., Singer, C. P., Peariso, K. L., Lin, S.-J., Schimdt, P. J., Fahrni, C. J., Culotta, V. C., Penner-Hahn, J. E., and O'Halloran, T. V. (1997) *Science 278*, 853−856.
27. Huffman, D. L., and O'Halloran, T. V. (2000) *J. Biol. Chem. 275*, 18611−18614.
28. Rae, T. D., Schmidt, P. J., Pufahl, R. A., Culotta, V. C., and O'Halloran, T. V. (1999) *Science 284*, 805−808.
29. Sambrook, J., Fritsch, E., and Maniatis, T. (1989) *Molecular Cloning: A Laboratory Manual*, Vols. 1−3, Cold Spring Harbor Laboratory Press, Cold Spring Harbor, NY.
30. Datsenko, K. A., and Wanner, B. L. (2000) *Proc. Natl. Acad. Sci. U.S.A. 97*, 6640−6645.
31. Ausubel, F. M., Brent, R., Kingston, R. E., Moore, D. D., Seidman, J. G., Smith, J. A., and Struhl, K. (1995) in *Current Protocols in Molecular Biology* (Janssen, Ed.) John Wiley and Sons, New York.
32. Bradford, M. M. (1976) *Anal. Biochem. 72*, 248−254.
33. Ames, G. F., Prody, C., and Kustu, S. (1984) *J. Bacteriol. 160*, 1181−1183.
34. Lehmann, H. P., Schosinsky, K. H., and Beeler, M. F. (1974) *Clin. Chem. 20*, 1564−1567.
35. Roth, E. F., Jr., and Gilbert, H. S. (1984) *Anal. Biochem. 137*, 50−53.
36. Fridovich, I. (1985) in *CRC Handbook of Methods for Oxygen Radical Research* (Greenwald, R. A., Ed.) pp 213−215, CRC Press, Boca Raton, FL.
37. Venters, R. A., Nelson, M. J., McLean, P., True, A. E., Levy, M. A., Hoffman, B. M., and Orme-Johnson, W. H. (1986) *J. Am. Chem. Soc. 108*, 3487−3498.
38. Werst, M. M., Davoust, C. E., and Hoffman, B. M. (1991) *J. Am. Chem. Soc. 113*, 1533−1538.
39. Davoust, C. E., Doan, P. E., and Hoffman, B. M. (1996) *J. Magn. Reson. A119*, 38−44.
40. Hoffman, B. M., DeRose, V. J., Ong, J.-L., and Davoust, C. E. (1994) *J. Magn. Reson., Ser. A 110*, 52−57.
41. Mims, W. B. (1965) *Proc. R. Soc. London A 283*, 452−457.
42. Doan, P. E., and Hoffman, B. M. (1997) *Chem. Phys. Lett. 269*, 208−214.
43. Fan, C., Doan, P. E., Davoust, C. E., and Hoffman, B. M. (1992) *J. Magn. Reson. 98*, 62−72.
44. Mims, W. B. (1984) *J. Magn. Reson. 59*, 291−306.
45. Hoffman, B. M., Martinsen, J., and Venters, R. A. (1984) *J. Magn. Reson. 59*, 110−123.
46. Hoffman, B. M., DeRose, V. J., Doan, P. E., Gurbiel, R. J., Houseman, A. L. P., and Telser, J. (1993) in *Biological Magnetic Resonance* (Berliner, L. J., and Reuben, J., Eds.) pp 151−218, Plenum, New York.
47. Gurbiel, R. J., Fann, Y. C., Surerus, K. K., Werst, M. M., Musser, S. M., Doan, P. E., Chan, S. I., Fee, J. A., and Hoffman, B. M. (1994) *J. Am. Chem. Soc. 115*, 10888−10894.
48. Doan, P. E. (1997) *GENSIM*, recently modified version of Gendor available on request from author Peter Doan at ped131@northwestern.edu.
49. Berks, B. C., Sargent, F., and Palmer, T. (2000) *Mol. Microbiol. 35*, 260−274.
50. Cristobal, S., de Gier, J. W., Nielsen, H., and von Heijne, G. (1999) *EMBO J. 18*, 2982−2990.
51. Peisach, J., and Blumberg, W. E. (1974) *Arch. Biochem. Biophys. 165*, 691−708.
52. McCord, J. M., and Fridovich, I. (1969) *J. Biol. Chem. 244*, 6049−6055.
53. Rotilio, G., Morpurgo, L., Giovagnoli, C., Calabrese, L., and Mondovi, B. (1972) *Biochemistry 11*, 2187−2192.
54. Atherton, N., and Horsewill, A. (1979) *J. Mol. Phys. 37*, 1349−1361.
55. Wertz, J. E., and Bolton, J. R. (1986) *Electron spin resonance: elementary theory and practical applications*, 2nd ed., Chapman & Hall, New York.
56. Peisach, J., Mims, W. B., and Davis, J. L. (1979) *J. Biol. Chem. 254*, 12379−12389.
57. McCracken, J., Pember, S., Benkovic, S. J., Vilafranca, J. J., Miller, R. J., and Peisach, J. (1988) *J. Am. Chem. Soc. 110*, 1069−1074.
58. Mims, W. B., and Peisach, J. J. (1978) *J. Chem. Phys. 69*, 4921−4930.
59. Jin, H., Thomann, H., Coyle, C. L., and Zumft, W. G. (1989) *J. Am. Chem. Soc. 111*, 4262−4269.
60. McCracken, J., Peisach, J., and Dooley, D. M. (1987) *J. Am. Chem. Soc. 109*, 4064−4072.
61. Flanagan, H. L., and Singel, D. J. (1987) *J. Chem. Phys. 87*, 5606−5616.
62. Flanagan, H. L., and Singel, D. J. (1988) *J. Chem. Phys. 89*, 2585−2586.
63. Holm, R. H., Kennepohl, P., and Solomon, E. I. (1996) *Chem. Rev. 96*, 2239−2314.
64. Surerus, K. K., Chen, M., Wim van der Zwann, J., Rusnak, F. M., Kolk, M., Duin, E. C., Albracht, S. P. J., and Munck, E. (1994) *Biochemistry 33*, 4980−4993.
65. Fann, Y.-C., Ahmed, I., Blackburn, N. J., Boswell, J. S., Verkhovskaya, M. L., Hoffman, B. M., and Wikstrom, M. (1995) *Biochemistry 34*, 10245−10255.
66. Adman, E. T. (1991) *Adv. Protein Chem. 42*, 145−197.
67. Huffman, D. L., and O'Halloran, T. V. (2001) *Annu. Rev. Biochem. 70*, 677−701.
68. Kitajima, N. (1992) *Adv. Inorg. Chem. 39*, 1−77.
69. Hoogstraten, C. G., Grant, C. V., Horton, T. E., DeRose, V. J., and Britt, R. D. (2002) *J. Am. Chem. Soc. 124*, 834−842.

BI0259960